THE JOURNAL OF PHYSICAL CHEMISTRY C

Article

pubs.acs.org/JPCC

Existence of Multiple Phases of Water at Nanotube Interfaces

Amir Barati Farimani and Narayana R. Aluru*

Department of Mechanical Science and Engineering, Beckman Institute for Advanced Science and Technology University of Illinois at Urbana−Champaign, Urbana, Illinois 61801, United States

Supporting Information

ABSTRACT: Water, because of its anomalous properties, can exhibit complex behavior under strong confinement. At room temperature and pressure, water is assumed to exist in a single phase as a liquid under confinement (e.g., in a carbon nanotube). In this study, using extensive molecular dynamics simulations, we show the existence of multiple phases of water when water meets a nanotube surface under atmospheric conditions (T = 300 K, P = 1 atm). Vapor, high-density ice, and liquid water phases coexist in the region within ∼1 nm from the surface. Structure factor, entropy, pressure, viscosity, and rotational diffusion of water layers near the surface reveal substantial phase anomalies induced by confinement. We show the presence of a new high-density solid-state ice layer (ρ = 3.9 g/cm^3) with rhombic structure coexisting adjacent to vapor and liquid water. The existence of multiple phases of water near an interface can explain, for example, the slip phenomena, self-filling behavior of a carbon nanotube, and fast transport of water.

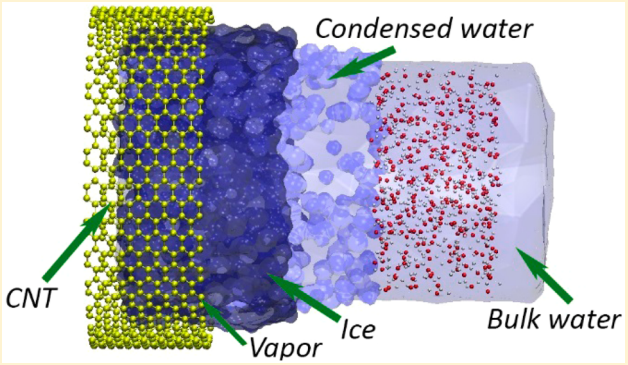

INTRODUCTION

Water exhibits many complex and anomalous properties in its bulk state. The behavior of water can be even more complex and anomalous under confinement.[1,2] For example, interesting effects such as anomalous phase behavior can be observed when the confined spaces approach the size of a few water molecules.[2−5] Surface forces in the 1 to 2 nm region from the wall introduce significant spatial effects that alter the density, viscosity, diffusion, entropy, and pressure of water.[6,7] These changes can lead to the creation of new water phases, namely, pentagonal and hexagonal ice structures inside an (8,8) carbon nanotube (CNT) and (9,9) CNT at room temperature.[2,8]

Confined water has been studied in various nanostructured systems including CNTs,[9−11] graphene[12] and MoS_2 nanopores,[13−15] aquaporins,[16] and buckyball.[17] As a result of these studies, intriguing applications such as water desalination,[13,14,18] fast water transport,[19] and nanoscale chip cooling have been discovered and explored.[16,20−22]

Bulk water exhibits several phases at different thermodynamic states.[23−25] Various types of ice,[26] observed in nature and in laboratories, differ in structure, density, and pressure.[26−28] In recent years, molecular dynamics (MD) simulations were performed to understand the fundamental phase behavior of water in confinement with the change in temperature and density.[1,29−36] Other studies have primarily focused on one layer of water (contact layer) near the wall and its phase change with pressure and density.[31,37] Water confined between two surfaces or in a pore can experience stronger structural changes when the confined region is comparable to the molecular size. For example, in CNTs with a diameter <0.8 nm, single file water with ∼1.5 hydrogen bonds (HBs) is observed.[7,38] For CNTs with diameters of 0.9 to 1.1 nm, water molecules form a pentagonal/hexagonal structure.[39] In larger diameter CNTs, fast transport of water is observed.[20,21] Given these interesting properties, with CNTs and other nanopores, it is possible to engineer a variety of water structures, even those not found in nature, at room temperature[21] by tuning the pore size and surface chemistry. Understanding the structure, dynamics, and thermodynamic properties of water phases in CNTs at room temperature can be helpful in understanding phase transition in nanoscale confinement of water. In recent work, the nature of phase transition of water in nanoscale confinement has been questioned.[29−31,37,40] Although several studies were performed to elucidate the nature of phase change in CNTs, most of them focused on the phase change with temperature,[41−43] and the spatial phase change (at room temperature, T = 300 K) in CNTs due to configurational entropy induced by confinement was not investigated in detail.[24−26] A systematic understanding of the effect of confinement on the complex spatial variation of the water phase and its properties, especially at room temperature, is currently lacking. Here, we show the existence of different phases of water in a single carbon nanotube at room temperature. Significant density oscillations in sub-2 nm CNTs result in multiphase structure of water. High density ice layer (HDL),[44,45] vapor,[30] and liquid water coexist in carbon

Received: June 17, 2016
Revised: September 28, 2016
Published: September 28, 2016

DOI: 10.1021/acs.jpcc.6b06156
J. Phys. Chem. C 2016, 120, 23763−23771

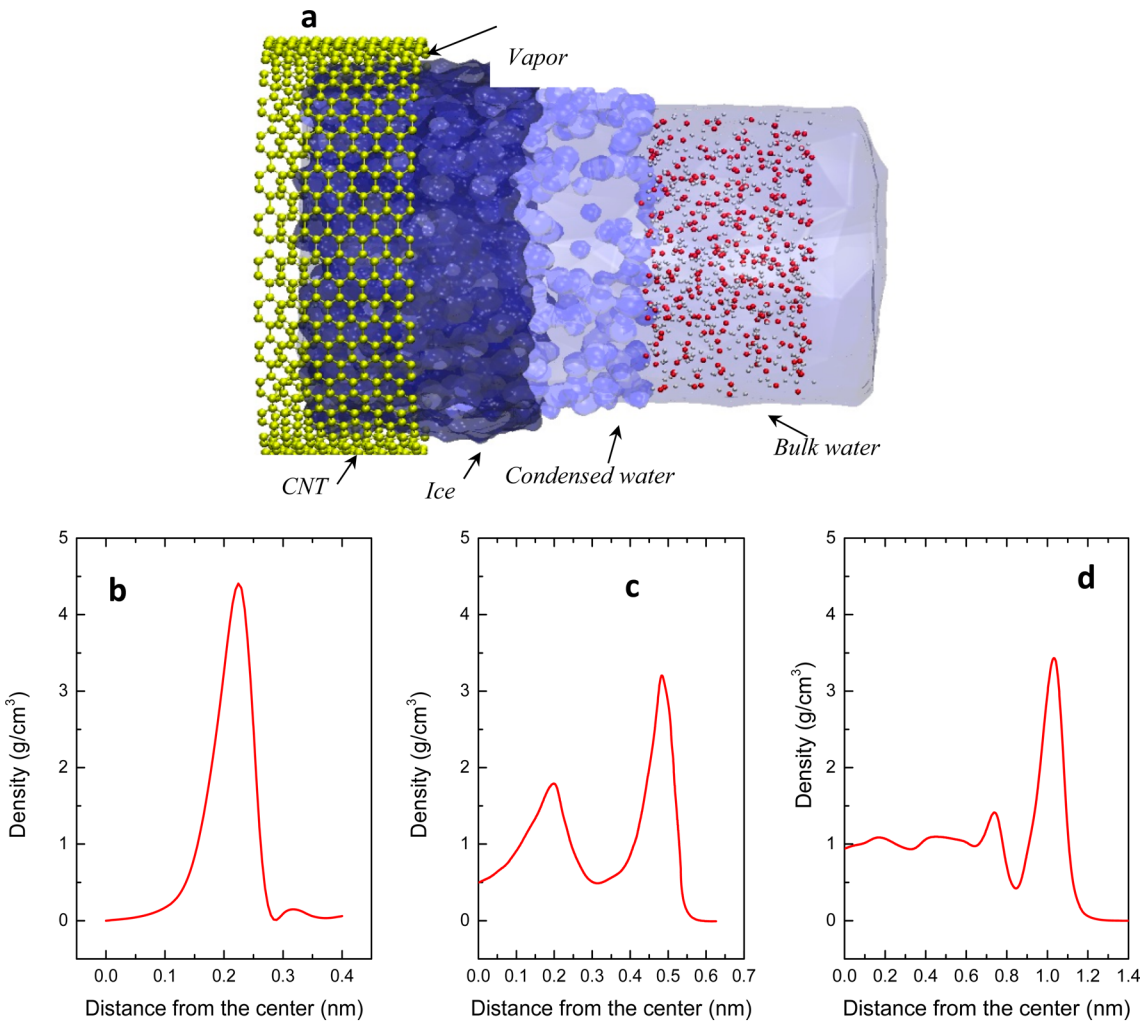

Figure 1. (a) Schematic of phase volume fraction and their arrangement inside a (30, 30) CNT. Spatial variation of density of water in a carbon nanotube obtained with MD: (b) (9,9) CNT, (c) (12,12) CNT, and (d) (20, 20) CNT.

nanotubes at room temperature (Figure 1a). Thin layer of ice-like solid (monolayer ice) has a density that is about three times higher than that of liquid water with gigapascals (GPa) pressure. We show that the volume fraction of different phases of water varies with the diameter of the nanotube. We also establish the physical foundations of the anomalous phase behavior of water in nanotube to the spatial phase inhomogeneity that exists at a distance of 1 nm near the wall.

METHODS

MD simulations were performed using LAMMPS.[46] A periodic boundary condition was applied in all directions for filling the carbon nanotubes. Temperature was maintained at 300 K by applying the Nosé−Hoover thermostat with a time constant of 0.1 ps. The Parinello−Rahman scheme with a time constant of 0.1 ps and compressibility of 4.5×10^5 bar $^{-1}$ was used to adjust the pressure of the system at 0.1 MPa. A simple point charge extended (SPC/E) model was used for water. Lennard-Jones (LJ) parameters for the carbon atoms are $\sigma = 0.339$ nm and $\varepsilon = 0.2897$ kJ/mol.[7] The SPC/E water model is used because its diffusion coefficient (2.59×10^{-5} cm^2/s) is closer to the experimental value (2.3×10^{-5} cm^2/s). The cutoff distance for the LJ interactions is 15 Å. The long-range electrostatic interactions were computed by using the particle mesh Ewald method (real space cutoff, 10 Å; reciprocal space gridding, 1.2 Å, fourth-order interpolation). The SHAKE algorithm was used to maintain the geometry of the water molecules. Initially, to ensure equal pressure in all tube sizes, the CNT with water inside was connected to two reservoirs at both ends, whose pressure was set to 1 atm. In all cases, the equilibrium density of the bulk reservoir was ∼1 g/cm^3. We run the simulation for 1 ns to ensure the equilibrium self-filling of carbon nanotubes. The reservoirs were then removed, and periodic boundary condition was imposed along the tube axis (see Supporting Information on CNT filling process). Carbon atoms were frozen to their lattice position to prevent out-of-plane displacement. MD studies on nanofluidic properties of CNTs under equilibrium conditions have shown that treating CNTs as rigid in their lattice is a reasonable approximation.[21] Because the quadrupole interaction has a negligible contribution to the density and water dipole moment,[47,48] we neglected the quadruple interaction in our calculations.

The error bars in the results are the standard deviations based on four different initial configurations. After equilibration, the simulations were run for an additional 15−20 ns. Results for density, pressure, configuration entropy, and structure factor were computed based on 10 fs sampling rate. To avoid entrance effects, only the middle part of the CNT was considered. Simulations contained 1000−18 000 water molecules depend-

DOI: 10.1021/acs.jpcc.6b06156
J. Phys. Chem. C 2016, 120, 23763−23771

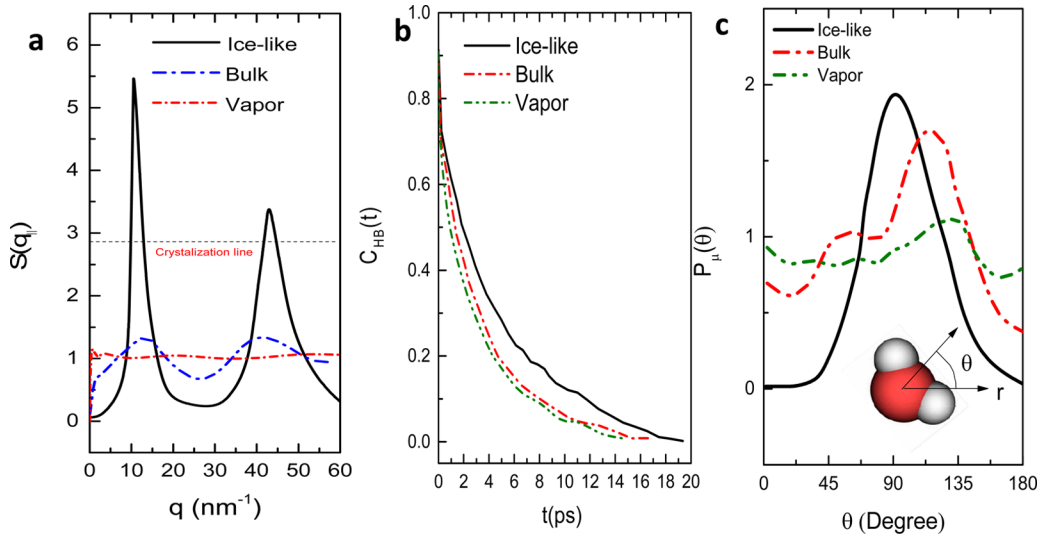

Figure 2. (a) In-plane structure factor of water molecules in different layers of water in a carbon nanotube. Structure factor shows peaks beyond the crystallization line for the high density layer (ice-like layer). (b) Hydrogen-bond lifetime computed in different layers and phases of (20,20) carbon nanotube. The decay characteristic of the hydrogen bond lifetime becomes slower as the density is higher. (c) Orientation of the water dipole distribution in different layers. In the ice-like layer, molecules have a strong orientation as the distribution has a peak.

ing on the size of each tube. All simulations were performed in the NVT ensemble.

For calculation of different entropy components, we used the 2PT method.[16,49,50] Isothermal calculation of viscosity showed that viscosity is a strong function of density.[51,52] The method for computing viscosity can be found in the Supporting Information. For characterizing the density phase diagram of water for different ranges of density, we analyzed the RDF and structure factor of water. We compare the structure factor of water with the Hansen–Verlet[53] criterion and the structure factor of ice *Ih*[24], bulk vapor, and liquid water to obtain the density phase diagram.

RESULTS AND DISCUSSION

We present results on (9,9), (12,12), and (20,20) carbon nanotubes. We simulated some other tube sizes and these are included in the analysis of the phase volume fraction. Density and all other spatially variant properties are obtained by cylindrical binning of the tubes. Density variations for three different tube sizes are shown in Figure 1. In the (20,20) CNT, a large portion of water has bulk density equal to 1 g/cm^3. As the diameter, *D*, of CNT decreases, the bulk core vanishes and density variations can be observed even in the center of the tube. In all density plots, we observe a high density peak with ρ > 2 g/cm^3. The spatial variation of density near the CNT wall is observed in all tube diameters. The region adjacent to the wall (within 1 Å) is the depletion region where 5–10% of bulk density can be found (Figure 1). The density layer with ρ > 2 g/cm^3 exists within a distance of ∼2 Å from the wall (Figure 1). In the (9,9) CNT, the two maximum density peaks overlap and a density peak >3 g/cm^3 is observed. (Figure 1c)

To characterize the multiphase structure of water in CNTs, we computed several structural/dynamical properties. We selected three regions inside the (20,20) CNT based on the density (Figure 1): 0 < *r* < 0.6 nm (bulk water), 0.95 < *r* < 1.1 nm (ice-like), and *r* > 1.1 nm (vapor) (*r* is the distance from the center of the CNT). In Figure 2a, we computed the structure factor of different layers in (20,20) CNT. To compute the in-plane structure factor, the in-plane radial distribution function $g_{\parallel}(r)$ for each layer is calculated. The in-plane radial distribution function can be obtained by "unrolling" the trajectories of the molecules from the cylindrical coordinates to Cartesian coordinates in the lateral direction.[22] By plugging $g_{\parallel}(r)$ in $S(q_{\parallel}) = 1 + \rho \int dr\, e^{-iqr}[g_{\parallel}(r) - 1]$, the in-plane structure factor is computed.[54] In Figure 2a, it can be observed that for the ice-like layer the peaks are beyond the water crystallization using the Hansen–Verlet criterion,[53] $S(q_{\parallel})$ > 2.85. Hansen–Verlet criterion discriminates between liquid and solid phases of matter based on the structure factor intensity.[53] On the basis of this, we can conclude that water is crystallized in the ice-like layer. In the structure factor for bulk vapor, no oscillation around $S(q_{\parallel}) = 1$ is observed. This is consistent with the structure factor of the vapor layer in the (20,20) CNT. The vapor layer $S(q_{\parallel})$ is a constant, nonoscillatory function (Figure 2a), which establishes the existence of vapor phase in the layer with *r* > 1.1 nm.[53] Han et al.[29] and Brovchenko et al.[30] developed density–temperature phase diagrams of water in confinement for densities (ρ < 1.0 g/cm^3) and showed that water with densities of ρ < 0.65 g/cm^3 is in vapor phase. For *r* > 1.1 nm, in (20,20) CNT, the density is lower than ρ < 0.65 g/cm^3.

Water HB dynamics is also a strong signature of water phase. For bulk water, the HB lifetime, $C_{HB}(t)$ is larger in ice compared with its liquid state.[55] In vapor state, because of the higher diffusion, the HBs are formed and broken more frequently, leading to a smaller $C_{HB}(t)$.[55] We analyzed the hydrogen-bond dynamics of water inside CNTs for different layers of interest. The intermittent hydrogen-bond correlation function, $C_{HB}(t)$ is defined as $C_{HB}(t) = \frac{\langle h(t)\cdot h(0)\rangle}{\langle h(0)^2\rangle}$, where $h(t)$ is the number of HBs at time *t* and $h(0)$ is the number of HBs at (t = 0 ps).[6] To count the number of HBs, the geometrical criterion of HB formation is used.[7] In Figure 2b, $C_{HB}(t)$ is illustrated for three different layers in (20,20) CNT. For the ice-like layer, the relaxation time is longer compared with bulk and vapor phases. For bulk water, the relaxation time is ∼13.4 ps, while in the ice-like layer, it is 18.96 ps. The HB lifetime is enhanced in the ice-like layer due to the high density of water

DOI: 10.1021/acs.jpcc.6b06156
J. Phys. Chem. C 2016, 120, 23763–23771

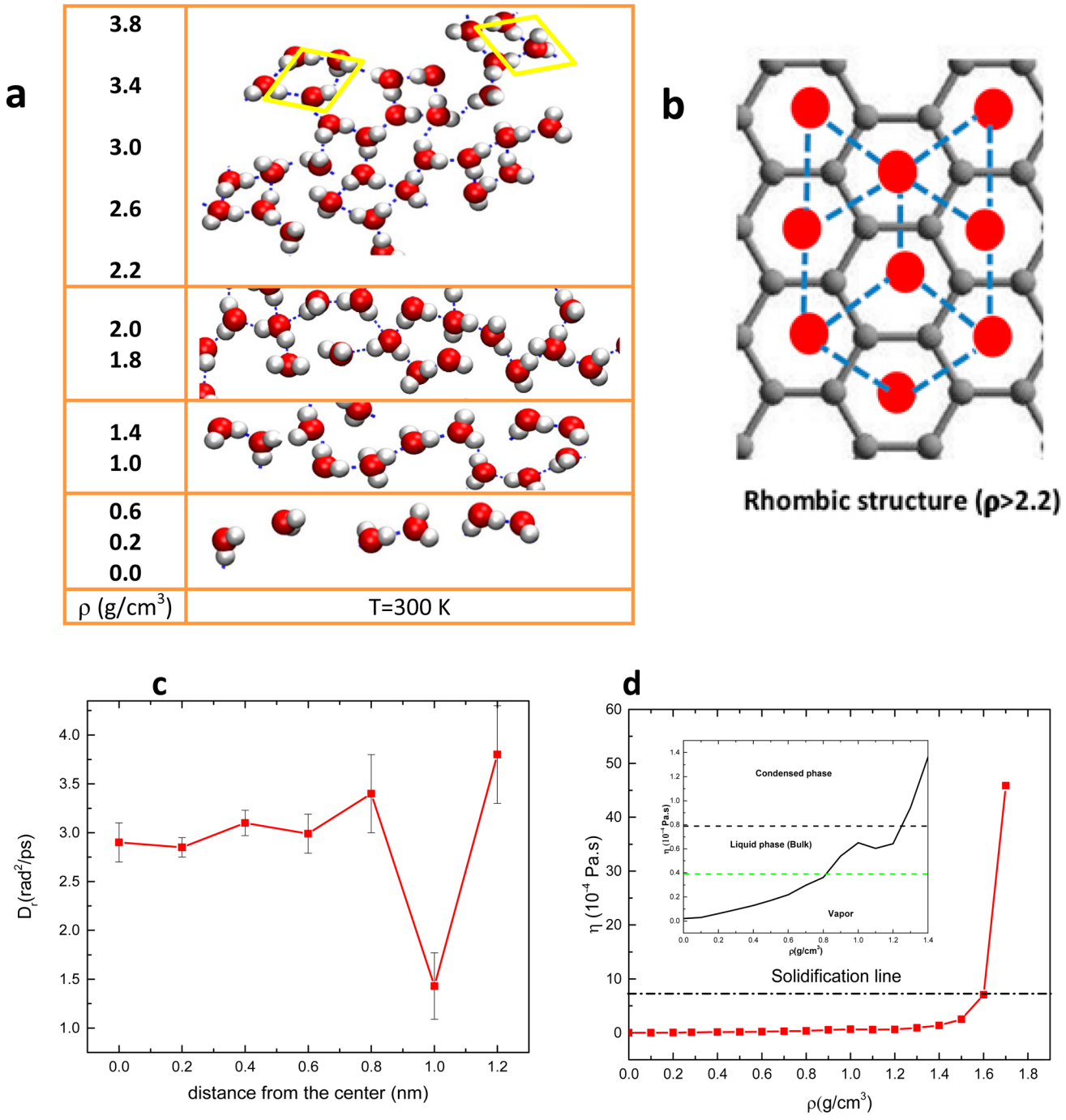

Figure 3. (a) $\rho-T$ = 300 K phase diagram of water in confinement (snapshots of different layers of water with different water structure and density; two samples of rhombic structure are depicted in yellow). (b) Rhombic structure of high density water for ρ > 2.2 g/cm^3 (dashed lines are representing the rhombic structure). (c) Spatial variation of the rotational diffusion coefficient of water. The rotational diffusion coefficient has a sharp drop in the first density layer (ice-like layer). (d) Variation of viscosity with density. For ρ > 1.6 g/cm^3, a jump in viscosity is observed that is due to the phase change from condensed water to ice. (The inset represents the enlarged viscosity changes for density range of 0.0 to 1.4 g/cm^3 and the viscosity for vapor phase and water.)

and a more pronounced water−water bonding. In contrast, in low-density water (vapor), HBs are broken at a faster rate.[6,55] The number of HBs near the wall (vapor region) is 1.8.[7] In bulk vapor, the average number of HBs is 2.4. In the vapor region adjacent to the wall (within 1 Å), water molecules that point toward the CNT wall could not make HBs; therefore, the number of HBs in this layer is reduced to 1.8, which is also consistent with the reduced number of HBs in bulk vapor. (The average HB in bulk vapor is 2.4.)

To obtain deeper insights into the structure of various phases of water inside a CNT, we investigate the water dipole orientations in the three layers. Figure 2c shows the distribution of the average water dipole orientation with respect to the radial direction for different phases. In the vapor region, the dipoles mainly have a flat distribution that is consistent with the bulk vapor phase ($0 < \theta < 180°$).[30] In the ice-like layer, the dipole has a preference (the dipole angle in radial direction has the angle, θ = 90°, for most of the simulation time) and is

DOI: 10.1021/acs.jpcc.6b06156
J. Phys. Chem. C 2016, 120, 23763−23771

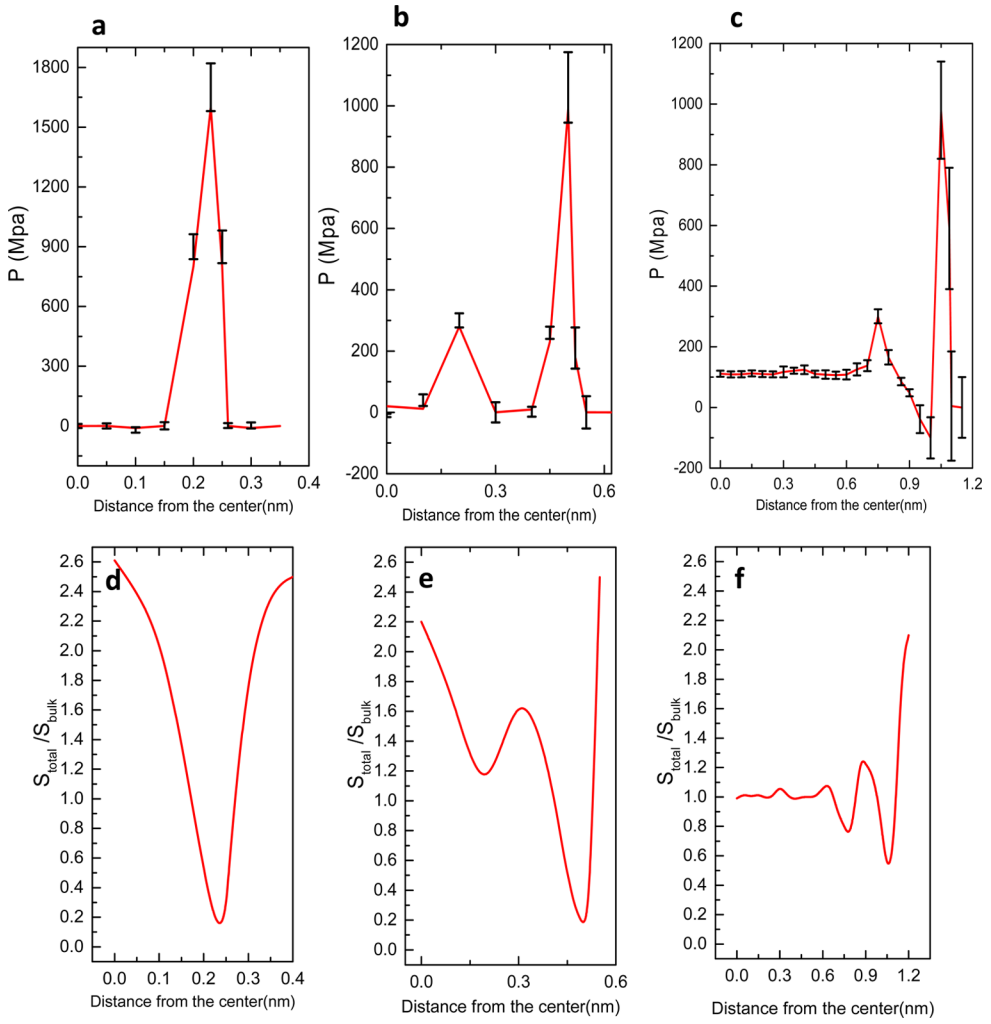

Figure 4. Spatial variation of pressure and entropy inside a carbon nanotube computed using MD. (a) Pressure in (9,9) CNT. (b) Pressure in (12,12) CNT. (c) Pressure in (20,20) CNT. (d) Spatial variation of normalized entropy in (9,9) CNT. (e) Spatial variation of normalized entropy in (12,12) CNT. (f) Spatial variation of normalized entropy in (20,20) CNT.

ordered (in all forms of bulk ice, the dipole of water molecule is also oriented).[29] In the bulk layer, neither a uniform nor a highly preferred dipole orientation is observed, which is typical of liquids.

To depict the structure of each layer in terms of water arrangement and clustering, we mapped the simulation trajectories onto a 2D plane. In Figure 3a, the most probable orientation of water and their clustering behavior versus density is shown. In the ice-like layer, we observed the rhombic ice structure.[29] The packing of the molecules in the rhombic structure gives rise to a density >3 g/cm^3. In Figure 3b, we show a graphical representation of water molecules with respect to the carbon nanotube rings in the lateral direction. Oxygen atoms are located in the center of the carbon rings and the O···H bond crosses the C−C bond.

To analyze the rotational dynamics of water molecules in different layers and phases, we computed the rotational diffusion coefficient along the radial direction. Figure 3c shows the rotational diffusion coefficient as a function of distance from the center of the (20,20) CNT. The calculation of the rotational diffusion coefficient[56] is explained in the Supporting Information. The rotational diffusion of water dipole in bulk is equal to 3.4 rad^2/ps. In the ice-like layer, rotational diffusion has the lowest value and is equal to 1.32 rad^2/ps. In this layer, the rotation of molecules is hindered because of the many-body pairwise potentials imposed from the CNT wall. In the vapor layer, the hydrogen bonding and density are lower, which gives the water molecules freedom to rotate. In this layer, the rotational diffusion is 3.95 rad^2/ps, which is larger compared with the bulk liquid water rotational diffusion (3.4 rad^2/ps). Our previous studies showed that the translational diffusion coefficient increases significantly in the vapor layer.[7]

Viscosity, Pressure, and Entropy of Phases. For confined water, viscosity is highly dependent on the density of the fluid. The layering of density in the radial direction gives rise to the variation of viscosity in the radial direction. To estimate the variation of viscosity in the radial direction, we performed multiple MD simulations of bulk water with different densities. The method used to calculate viscosity is explained in the SI. Figure 3d shows the variation of viscosity with density. For ρ > 1.6 g/cm^3, a jump in viscosity is observed that confirms the solidification of water for densities >1.6 g/cm^3. For ρ < 0.8 g/cm^3, viscosity behavior is very similar to the viscosity of water vapor. By comparing Figures 1 and 3d, viscosity variation of water inside the CNT can be estimated. In the high-density layer (ice-like), viscosity is several orders of magnitude higher than that of bulk water.

DOI: 10.1021/acs.jpcc.6b06156
J. Phys. Chem. C 2016, 120, 23763−23771

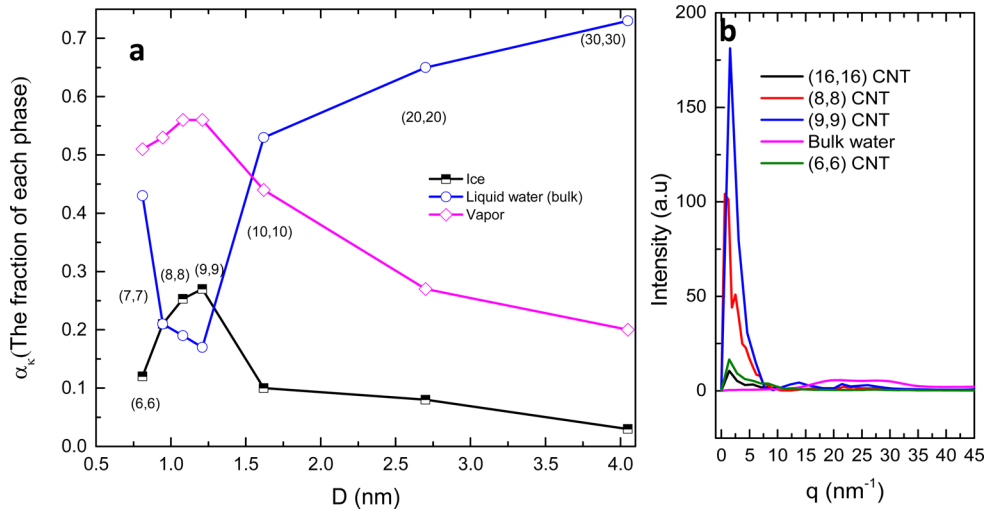

Figure 5. (a) Volume fraction of phases (α_K) of water for CNTs of different diameters (D). CNTs contain several phases of water. (b) Total structure factor of bulk liquid water, (6,6) CNT, (8,8) CNT, (9,9) CNT, and (16,16) CNT. Sharp peaks in (8,8) CNT and (9,9) CNT indicate the presence of ice-like structures. Small peaks observed for (6,6) CNT and (16,16) CNT indicate $\alpha_{ice} \approx 10\%$.

Han et al.[29] obtained the $\rho-T$ phase diagram of water in confinement by MD simulations. According to this phase diagram, for the thermodynamic states of $\rho > 1.35$ g/cm^3 and $T = 230$ K, rhombic ice structure is observed for the entire water inside the slit (with 2 nm). We note that we observed the same structure for the high-density layer (ice-like layer) for thermodynamic states corresponding to $\rho > 1.6$ g/cm^3 and $T = 300$ K. The most evident/clear rhombic structures are observed for $\rho > 2.2$ g/cm^3 within the ice-like layer. For the densities ranging from 1.6 to 2.2 g/cm^3,[24] characteristics (structure factor, pressure, entropy) are very similar to the behavior of gels (mushy zone) or of a mixture of super cooled water and low density layer (LDL).[28,57] We also observed continuous phase transition occurring spatially in the radial direction. Although the structure factor of this region has sharp peaks ($S(q_\parallel)_{max} = 2.11$), they do not exceed the crystallization point defined by the Hansen–Verlet criterion[53] ($S(q_\parallel) > 2.85$).

To investigate the phase properties in more detail, we computed the spatial variation of pressure and entropy inside CNTs. Pressure is computed by considering the ideal gas and virial contributions, $P = \frac{Nk_BT}{V} - \frac{1}{DV}\langle\sum_i \sum_{i>j} r_{ij}\cdot F_{ij}\rangle$, $D = 3$, N/V is density, V is volume, and F_{ij} is the force between atoms i and j separated by the distance r_{ij}. In Figure 4a–c, the spatial variation of pressure, computed with MD, is presented. In the ice-like layer, pressure approaches a few gigapascals. Isothermal pressure–density diagrams predict ice VII and VIII structures for the equivalent pressure–density range of the ice-like layer.[58] The commonly used isothermal pressure–density equation of state $\left(\frac{P}{P_{bulk}} = 3000\left(\frac{\rho}{\rho_{bulk}}\right)^7 - 3000\right)$ predicts a huge increase in the pressure with a small perturbation in density.[59] MD simulations for isotherms at $T = 300$ K show that the change in density (from $\rho = 1.0$ to 1.1 g/cm^3) would change pressure from 1 to 200 MPa. Poole et al. found that at ($\rho = 1.47$ g/cm^3, $T = 300$ K), and the pressure corresponds to 2000 MPa.[59] In the vapor layer, the pressure is very low, which corresponds to the rarified water vapor phase.

We computed the spatial variation of the total entropy of water in CNT. To estimate the total entropy in each layer, we used the 2PT method to obtain the different components of the total entropy.[16] The 2PT method decomposes the entropy into translational, rotational, and vibrational components ($S_{total} = S_{trans} + S_{rot} + S_{vib}$). The rigid water model gives $S_{vib} = 0$. (In practice, the contribution of S_{vib} is <1 J/mol·K.) The method for computation of entropy with the 2PT method is explained in the Supporting Information. Our calculation of entropy of bulk water shows a 4% error compared with experiments. Figure 4d–f shows the spatial distribution of total entropy from MD. In the ice-like layer, entropy is minimum inside the CNT and is about 0.3 to 0.5 times the bulk value, S_{bulk}. The entropy change from bulk to the ice-like layer is equal to the entropy of water solidification (icing). Near the wall (within 1 Å distance from the CNT wall), entropy is about 2.5 to 3 times the bulk entropy (bulk water entropy calculated using the 2PT method is ~61 J/mol·K), which agrees with the vapor phase entropy.

To investigate the coexistence of different phases in CNTs, we analyzed CNTs with different diameter (D) and their phase volume fractions. Interesting phase fractions can be observed for diameters <2 nm. Figure 5a depicts the volume fraction of phases (α_K) for CNTs with different diameters, D. We computed the volume fraction based on the ratio of the volume of each phase divided by the total volume of the CNT. Volume of each phase in a region is defined based on the density–phase diagram (i.e., $0 < \rho < 0.65$ g/cm^3: vapor; $0.65 < \rho < 2.2$ g/cm^3: bulk water; and $\rho > 2.2$ g/cm^3: ice). For (8,8) and (9,9) CNTs, the ice volume fraction is >30% and pentagonal and hexagonal ice structure is observed. To investigate the ice structure of (8,8) and (9,9) CNTs, we present the total structure factor of CNTs of different diameters in Figure 5b. The total structure factor shows high peaks for these two CNTs. For other CNTs, the ice volume fraction of phases is <10% and is reflected as low intensity wave numbers in the structure factor. It is also notable that increase in energy term of LJ potential in water–C interaction will increase the volume fraction of ice and vapor for a few percent. In Figure 5a, as the diameter increases, bulk water volume fraction increases. It can be estimated that for $D = 1.0$ μm, 99.8% is liquid water.

Isothermal Phase Diagram of Water in Carbon Nanotubes. To investigate the isothermal phase diagram of water in carbon nanotubes, we computed the structure factor and RDF of layers with different densities. On the basis of the

DOI: 10.1021/acs.jpcc.6b06156
J. Phys. Chem. C 2016, 120, 23763–23771

characteristics of structure factor peaks and the criterion introduced by a Hansen–Verlet,[53] we defined the phases and phase lines. We averaged the phase properties (pressure, entropy) for the corresponding density points in a number of carbon nanotubes with diameters ranging from 0.8 to 4 nm (for example, we averaged the corresponding pressure and entropy for a density of 0.8 g/cm^3 in (6,6) CNT, (7,7) CNT, etc.). The corresponding phase diagram is shown in Figure 6a. In general, as density increases, pressure increases significantly and the change in entropy with density has a near-linear nature.

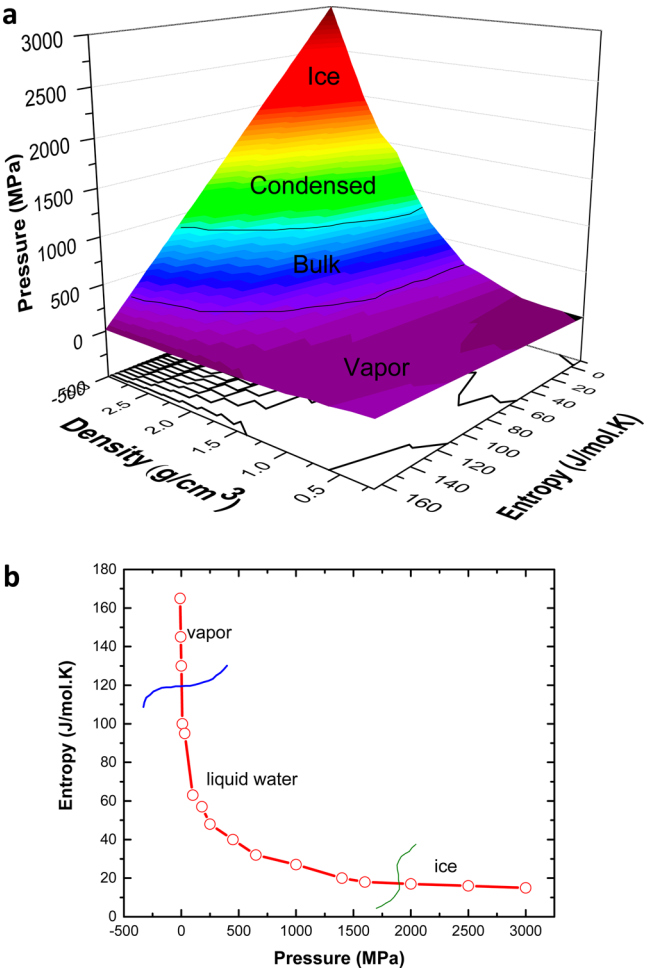

Figure 6. (a) Phase diagram of water in carbon nanotubes. Vapor region is where the entropy is high and density is low. As entropy decreases to 20 J/mol·K and pressure is on the order of gigapascals, the ice phase appears. (b) Entropy–pressure phase diagram of water in all CNTs.

To investigate the change in the entropy of water with pressure, we computed the entropy–pressure phase diagram (see Figure 6b) using the same method that was used in Figure 6a. As pressure increases to high values of ~2000 MPa, the entropy reduces to ~20 J/mol·K. The entropy curve is continuous with respect to pressure even at the phase change points, which implies that the type of phase change is continuous.

CONCLUSIONS

We conclude that water has a multiphase structure in carbon nanotubes with diameters less than 2 to 3 nm. The ice-like layer is one molecule thick with an ordered rhombic monolayer structure that exists near the wall. A vapor (dilute water) phase exists between the ice-like layer and the wall. In CNTs with diameter <1.2 nm, the existence of bulk liquid water is rare and the combination of ice and vapor phases is observed. Confined water can exhibit a continuous phase change over intermolecular distances from the wall. The ice-like layer has the lowest entropy and highest possible pressure and density. We also conclude that nanometer confinement of water can induce the continuous phase change from liquid phase to ice and vapor within 1 nm.

ASSOCIATED CONTENT

Supporting Information

The Supporting Information is available free of charge on the ACS Publications website at DOI: 10.1021/acs.jpcc.6b06156.

Methods for computing rotational diffusion coefficient, entropy, viscosity, and also the methodology to fill the CNT with water. (PDF)

AUTHOR INFORMATION

Corresponding Author

*E-mail: aluru@illinois.edu.

Notes

The authors declare no competing financial interest.

ACKNOWLEDGMENTS

This work is supported by AFOSR under grant # FA9550-12-1-0464 and by NSF under grants 1506619, 1420882, and 1545907. We also thank Ravi Bhadauria for the fruitful discussions on viscosity calculations. We gratefully acknowledge the use of the parallel computing resource Blue Waters provided by the University of Illinois and National Center for Supercomputing Applications (NCSA).

REFERENCES

(1) Koga, K.; Gao, G. T.; Tanaka, H.; Zeng, X. C. Formation of Ordered Ice Nanotubes inside Carbon Nanotubes. *Nature* **2001**, *412*, 802–805.

(2) Mashl, R. J.; Joseph, S.; Aluru, N. R.; Jakobsson, E. Anomalously Immobilized Water: A New Water Phase Induced by Confinement in Nanotubes. *Nano Lett.* **2003**, *3*, 589–592.

(3) Chaban, V. V.; Prezhdo, O. V. Water Boiling inside Carbon Nanotubes: Toward Efficient Drug Release. *ACS Nano* **2011**, *5*, 5647–5655.

(4) Vaitheeswaran, S.; Yin, H.; Rasaiah, J. C.; Hummer, G. Water Clusters in Nonpolar Cavities. *Proc. Natl. Acad. Sci. U. S. A.* **2004**, *101*, 17002–17005.

(5) Ferguson, A. L.; Giovambattista, N.; Rossky, P. J.; Panagiotopoulos, A. Z.; Debenedetti, P. G. A Computational Investigation of the Phase Behavior and Capillary Sublimation of Water Confined between Nanoscale Hydrophobic Plates. *J. Chem. Phys.* **2012**, *137*, 144501.

(6) Hanasaki, I.; Nakatani, A. Hydrogen Bond Dynamics and Microscopic Structure of Confined Water inside Carbon Nanotubes. *J. Chem. Phys.* **2006**, *124*, 174714.

(7) Farimani, A. B.; Aluru, N. R. Spatial Diffusion of Water in Carbon Nanotubes: From Fickian to Ballistic Motion. *J. Phys. Chem. B* **2011**, *115*, 12145–12149.

(8) Takaiwa, D.; Koga, K.; Tanaka, H. Structures of Filled Ice Nanotubes inside Carbon Nanotubes. *Mol. Simul.* **2007**, *33*, 127–132.

(9) Calixte, E. I.; Samoylova, O. N.; Shuford, K. L. Confinement and Surface Effects of Aqueous Solutions within Charged Carbon Nanotubes. *Phys. Chem. Chem. Phys.* **2016**, *18*, 12204–12212.

DOI: 10.1021/acs.jpcc.6b06156
J. Phys. Chem. C 2016, 120, 23763–23771

(10) Wang, G. J.; Hadjiconstantinou, N. G. Why Are Fluid Densities So Low in Carbon Nanotubes? *Phys. Fluids* **2015**, *27*, 052006.
(11) Hummer, G.; Rasaiah, J. C.; Noworyta, J. P. Water Conduction through the Hydrophobic Channel of a Carbon Nanotube. *Nature* **2001**, *414*, 188−190.
(12) Foroutan, M.; Fatemi, S. M.; Shokouh, F. Graphene Confinement Effects on Melting/Freezing Point and Structure and Dynamics Behavior of Water. *J. Mol. Graphics Modell.* **2016**, *66*, 85−90.
(13) Suk, M. E.; Aluru, N. R. Water Transport through Ultrathin Graphene. *J. Phys. Chem. Lett.* **2010**, *1*, 1590−1594.
(14) Heiranian, M.; Farimani, A. B.; Aluru, N. R. Water Desalination with a Single-Layer Mos2 Nanopore. *Nat. Commun.* **2015**, *6*, 8616.
(15) Farimani, A. B.; Min, K.; Aluru, N. R. DNA Base Detection Using a Single-Layer Mos2. *ACS Nano* **2014**, *8*, 7914−7922.
(16) Farimani, A. B.; Aluru, N. R.; Tajkhorshid, E. Thermodynamic Insight into Spontaneous Hydration and Rapid Water Permeation in Aquaporins. *Appl. Phys. Lett.* **2014**, *105*, 83702−83702.
(17) Farimani, A. B.; Wu, Y. B.; Aluru, N. R. Rotational Motion of a Single Water Molecule in a Buckyball. *Phys. Chem. Chem. Phys.* **2013**, *15*, 17993−18000.
(18) Wang, E. N.; Karnik, R. Water Desalination Graphene Cleans up Water. *Nat. Nanotechnol.* **2012**, *7*, 552−554.
(19) Farimani, A. B.; Heiranian, M.; Aluru, N. R. Nano-Electro-Mechanical Pump: Giant Pumping of Water in Carbon Nanotubes. *Sci. Rep.* **2016**, *6*, 26211.
(20) Holt, J. K.; Park, H. G.; Wang, Y. M.; Stadermann, M.; Artyukhin, A. B.; Grigoropoulos, C. P.; Noy, A.; Bakajin, O. Fast Mass Transport through Sub-2-Nanometer Carbon Nanotubes. *Science* **2006**, *312*, 1034−1037.
(21) Joseph, S.; Aluru, N. R. Why Are Carbon Nanotubes Fast Transporters of Water? *Nano Lett.* **2008**, *8*, 452−458.
(22) Falk, K.; Sedlmeier, F.; Joly, L.; Netz, R. R.; Bocquet, L. Molecular Origin of Fast Water Transport in Carbon Nanotube Membranes: Superlubricity Versus Curvature Dependent Friction. *Nano Lett.* **2010**, *10*, 4067−4073.
(23) Poole, P. H.; Sciortino, F.; Essmann, U.; Stanley, H. E. Phase-Behavior of Metastable Water. *Nature* **1992**, *360*, 324−328.
(24) Harrington, S.; Zhang, R.; Poole, P. H.; Sciortino, F.; Stanley, H. E. Liquid-Liquid Phase Transition: Evidence from Simulations. *Phys. Rev. Lett.* **1997**, *78*, 2409−2412.
(25) Guissani, Y.; Guillot, B. A Computer-Simulation Study of the Liquid-Vapor Coexistence Curve of Water. *J. Chem. Phys.* **1993**, *98*, 8221−8235.
(26) Perez-Diaz, J. L.; Alvarez-Valenzuela, M. A.; Rodriguez-Celis, F. Surface Freezing of Water. *SpringerPlus* **2016**, *5*, 629.
(27) Mishima, O.; Stanley, H. E. The Relationship between Liquid, Supercooled and Glassy Water. *Nature* **1998**, *396*, 329−335.
(28) Debenedetti, P. G. Supercooled and Glassy Water. *J. Phys.: Condens. Matter* **2003**, *15*, R1669−R1726.
(29) Han, S.; Choi, M. Y.; Kumar, P.; Stanley, H. E. Phase Transitions in Confined Water Nanofilms. *Nat. Phys.* **2010**, *6*, 685−689.
(30) Brovchenko, I.; Geiger, A.; Oleinikova, A. Water in Nanopores: Ii. The Liquid-Vapour Phase Transition near Hydrophobic Surfaces. *J. Phys.: Condens. Matter* **2004**, *16*, S5345−S5370.
(31) Brovchenko, I.; Geiger, A.; Oleinikova, A.; Paschek, D. Phase Coexistence and Dynamic Properties of Water in Nanopores. *Eur. Phys. J. E: Soft Matter Biol. Phys.* **2003**, *12*, 69−76.
(32) Koga, K.; Zeng, X. C.; Tanaka, H. Effects of Confinement on the Phase Behavior of Supercooled Water. *Chem. Phys. Lett.* **1998**, *285*, 278−283.
(33) Tanaka, H. Thermodynamic Anomaly and Polyamorphism of Water. *Europhys. Lett.* **2000**, *50*, 340−346.
(34) Kaneko, T.; Bai, J.; Yasuoka, K.; Mitsutake, A.; Zeng, X. C. New Computational Approach to Determine Liquid-Solid Phase Equilibria of Water Confined to Slit Nanopores. *J. Chem. Theory Comput.* **2013**, *9*, 3299−3310.
(35) Lu, Q.; Straub, J. E. Freezing Transitions of Nanoconfined Coarse-Grained Water Show Subtle Dependence on Confining Environment. *J. Phys. Chem. B* **2016**, *120*, 2517−2525.
(36) Bordin, J. R.; Krott, L. B.; Barbosa, M. C. Surface Phase Transition in Anomalous Fluid in Nanoconfinement. *J. Phys. Chem. C* **2014**, *118*, 9497−9506.
(37) Giovambattista, N.; Rossky, P. J.; Debenedetti, P. G. Phase Transitions Induced by Nanoconfinement in Liquid Water. *Phys. Rev. Lett.* **2009**, *102*, 050603.
(38) Berezhkovskii, A.; Hummer, G. Single-File Transport of Water Molecules through a Carbon Nanotube. *Phys. Rev. Lett.* **2002**, *89*, 064503.
(39) Kolesnikov, A. I.; Zanotti, J. M.; Loong, C. K.; Thiyagarajan, P.; Moravsky, A. P.; Loutfy, R. O.; Burnham, C. J. Anomalously Soft Dynamics of Water in a Nanotube: A Revelation of Nanoscale Confinement. *Phys. Rev. Lett.* **2004**, *93*, 035503.
(40) Zhao, W. H.; Bai, J.; Yuan, L. F.; Yang, J. L.; Zeng, X. C. Ferroelectric Hexagonal and Rhombic Monolayer Ice Phases. *Chem. Sci.* **2014**, *5*, 1757−1764.
(41) Chang, X.; Li, H. C.; Fa, W. Double-Walled Ice Nanotubes Grown in Carbon Nanotubes: Molecular Dynamics Simulations. *J. Appl. Phys.* **2013**, *114*, 074314.
(42) Javadian, S.; Taghavi, F.; Yari, F.; Hashemianzadeh, S. M. Phase Transition Study of Confined Water Molecules inside Carbon Nanotubes: Hierarchical Multiscale Method from Molecular Dynamics Simulation to Ab Initio Calculation. *J. Mol. Graphics Modell.* **2012**, *38*, 40−49.
(43) Mochizuki, K.; Koga, K. Solid-Liquid Critical Behavior of Water in Nanopores. *Proc. Natl. Acad. Sci. U. S. A.* **2015**, *112*, 8221−8226.
(44) Giovambattista, N.; Stanley, H. E.; Sciortino, F. Phase Diagram of Amorphous Solid Water: Low-Density, High-Density, and Very-High-Density Amorphous Ices. *Phys. Rev. E* **2005**, *72*, 031510.
(45) Bellissentfunel, M. C.; Teixeira, J.; Bosio, L. Structure of High-Density Amorphous Water 0.2. Neutron-Scattering Study. *J. Chem. Phys.* **1987**, *87*, 2231−2235.
(46) Plimpton, S. Fast Parallel Algorithms for Short-Range Molecular-Dynamics. *J. Comput. Phys.* **1995**, *117*, 1−19.
(47) Werder, T.; Walther, J. H.; Jaffe, R. L.; Halicioglu, T.; Koumoutsakos, P. On the Water-Carbon Interaction for Use in Molecular Dynamics Simulations of Graphite and Carbon Nanotubes. *J. Phys. Chem. B* **2003**, *107*, 1345−1352.
(48) Werder, T.; Walther, J. H.; Jaffe, R. L.; Halicioglu, T.; Noca, F.; Koumoutsakos, P. Molecular Dynamics Simulation of Contact Angles of Water Droplets in Carbon Nanotubes. *Nano Lett.* **2001**, *1*, 697−702.
(49) Lin, S. T.; Maiti, P. K.; Goddard, W. A. Two-Phase Thermodynamic Model for Efficient and Accurate Absolute Entropy of Water from Molecular Dynamics Simulations. *J. Phys. Chem. B* **2010**, *114*, 8191−8198.
(50) Kumar, H.; Mukherjee, B.; Lin, S.-T.; Dasgupta, C.; Sood, A. K.; Maiti, P. K. Thermodynamics of Water Entry in Hydrophobic Channels of Carbon Nanotubes. *J. Chem. Phys.* **2011**, *134*, 124105.
(51) Bhadauria, R.; Aluru, N. R. A Quasi-Continuum Hydrodynamic Model for Slit Shaped Nanochannel Flow. *J. Chem. Phys.* **2013**, *139*, 074109.
(52) Woodcock, L. V. Equation of State for the Viscosity of Lennard-Jones Fluids. *AIChE J.* **2006**, *52*, 438−446.
(53) Hansen, J. P.; Verlet, L. Phase Transitions of Lennard-Jones System. *Phys. Rev.* **1969**, *184*, 151.
(54) Krott, L. B.; Barbosa, M. C. Anomalies in a Waterlike Model Confined between Plates. *J. Chem. Phys.* **2013**, *138*, 084505.
(55) Luzar, A.; Chandler, D. Hydrogen-Bond Kinetics in Liquid Water. *Nature* **1996**, *379*, 55−57.
(56) Debnath, A.; Mukherjee, B.; Ayappa, K. G.; Maiti, P. K.; Lin, S. T. Entropy and Dynamics of Water in Hydration Layers of a Bilayer. *J. Chem. Phys.* **2010**, *133*, 174704.
(57) Bellissent-Funel, M. C. Is There a Liquid-Liquid Phase Transition in Supercooled Water? *Europhys. Lett.* **1998**, *42*, 161−166.

DOI: 10.1021/acs.jpcc.6b06156
J. Phys. Chem. C 2016, 120, 23763−23771

(58) Kuhs, W. F.; Finney, J. L.; Vettier, C.; Bliss, D. V. Structure and Hydrogen Ordering in Ice-Vi, Ice-Vii, and Ice-Viii by Neutron Powder Diffraction. *J. Chem. Phys.* **1984**, *81*, 3612−3623.
(59) Harrington, S.; Poole, P. H.; Sciortino, F.; Stanley, H. E. Equation of State of Supercooled Water Simulated Using the Extended Simple Point Charge Intermolecular Potential. *J. Chem. Phys.* **1997**, *107*, 7443−7450.

DOI: 10.1021/acs.jpcc.6b06156
J. Phys. Chem. C 2016, 120, 23763−23771